Clim. Past, 14, 1805–1817, 2018
https://doi.org/10.5194/cp-14-1805-2018

Climate of the Past
Open Access
EGU

Hydroclimatic variations in southeastern China during the 4.2 ka event reflected by stalagmite records

Haiwei Zhang[1,2], Hai Cheng[1,3], Yanjun Cai[2,1,6], Christoph Spötl[4], Gayatri Kathayat[1], Ashish Sinha[5], R. Lawrence Edwards[3], and Liangcheng Tan[2,1,6]

[1]Institute of Global Environmental Change, Xi'an Jiaotong University, Xi'an 710054, China
[2]Institute of Earth Environment, Chinese Academy of Sciences, State Key Laboratory of Loess and Quaternary Geology, Xi'an 710061, China
[3]Department of Earth Sciences, University of Minnesota, Minneapolis, Minnesota 55455, USA
[4]Institute of Geology, University of Innsbruck, Innsbruck 6020, Austria
[5]Department of Earth Science, California State University Dominguez Hills, Carson, California 90747, USA
[6]Open Studio for Oceanic-Continental Climate and Environment Changes, Pilot National Laboratory for Marine Science and Technology (Qingdao), Qingdao 266061, China

Correspondence: Haiwei Zhang (zhanghaiwei@xjtu.edu.cn)

Received: 24 August 2018 – Discussion started: 30 August 2018
Accepted: 7 November 2018 – Published: 27 November 2018

Abstract. Although the collapses of several Neolithic cultures in China are considered to have been associated with abrupt climate change during the 4.2 ka BP event (4.2–3.9 ka BP), the timing and nature of this event and the spatial distribution of precipitation between northern and southern China are still controversial. The hydroclimate of this event in southeastern China is still poorly known, except for a few published records from the lower reaches of the Yangtze River. In this study, a high-resolution record of monsoon precipitation between 5.3 and 3.57 ka BP based on a stalagmite from Shennong Cave, Jiangxi Province, southeast China, is presented. Coherent variations in $\delta^{18}O$ and $\delta^{13}C$ reveal that the climate in this part of China was dominantly wet between 5.3 and 4.5 ka BP and mostly dry between 4.5 and 3.57 ka BP, interrupted by a wet interval (4.2–3.9 ka BP). A comparison with other records from monsoonal China suggests that summer monsoon precipitation decreased in northern China but increased in southern China during the 4.2 ka BP event. We propose that the weakened East Asian summer monsoon controlled by the reduced Atlantic Meridional Overturning Circulation resulted in this contrasting distribution of monsoon precipitation between northern and southern China. During the 4.2 ka BP event the rain belt remained longer at its southern position, giving rise to a pronounced humidity gradient between northern and southern China.

1 Introduction

The 4.2 ka BP event was a pronounced climate event in the Holocene that has been widely studied in the past 20 years. It was identified as an abrupt (mega)drought and/or cooling event in a variety of natural archives including ice cores, speleothems, lake sediments, marine sediments and loess. This climate episode was associated with the collapse of several ancient civilizations and human migrations in many sites worldwide (e.g., Egypt, Greece, the Indus Valley and the Yangtze Valley) (Weiss et al., 1993; Cullen et al., 2000; Gasse, 2000; DeMenocal, 2001; Weiss and Bradley, 2001; Thompson et al., 2002; Booth et al., 2005; Bar-Matthews and Ayalon, 2011; Berkelhammer et al., 2012; Ruan et al., 2016; Railsback et al., 2018). Recently, the 4.2 ka BP event was defined as the lower boundary of the Meghalayan stage by the International Commission on Quaternary Stratigraphy. The timing of this geological boundary was defined at a specific level (i.e., the transformation from calcite to aragonite accompanied by an abrupt increase in $\delta^{18}O$) in a stalagmite from northeast India (Walker et al., 2018).

The abrupt climate change associated with the 4.2 ka BP event has been proposed to have contributed to the collapses of Neolithic cultures in China (Jin and Liu, 2002; Huang et al., 2010, 2011; Zhang et al., 2010; Liu and Feng, 2012; Wu et al., 2017). Most of these studies imply a temperature drop

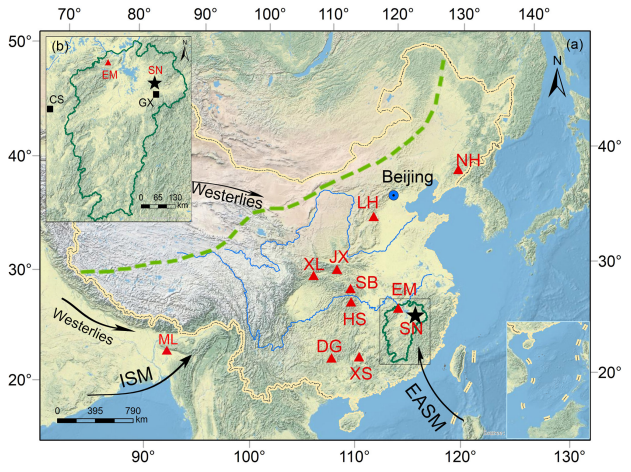

Figure 1. Location of Shennong Cave (SN, black star) and other caves mentioned in the paper. Panel **(a)** is an overview topographic map and Jiangxi Province is framed by the green line. Red triangles show the locations of published stalagmite records. NH: Nuanhe Cave (Tan, 2005), LH: Lianhua Cave (Dong et al., 2015), JX: Jiuxian Cave (Cai et al., 2010), XL: Xianglong Cave (Tan et al., 2018a), SB: Sanbao Cave (Dong et al., 2010), HS: Heshang Cave (Hu et al., 2008), EM: E'mei Cave (Zhang et al., 2018), XS: Xiangshui Cave (Zhang et al., 2004), DG: Dongge Cave (Wang et al., 2005), ML: Mawmluh Cave (Berkelhammer et al., 2012). Black arrows denote the directions of the East Asian summer monsoon (EASM), Indian summer monsoon (ISM) and westerlies, which affect the climate in China. The green dashed line indicates the limit of the modern East Asian summer monsoon. Panel **(b)** is an enlarged map showing the locations of Shennong Cave, the Guixi meteorological station (GX) and the GNIP station in Changsha (CS). The base map is the Natural Earth physical map at 1.24 km per pixel for the world (data source: US National Park Service, http://goto.arcgisonline.com/maps/World_Physical_Map; last access: 11 February 2017). For interpretation of the references to colors in this figure legend, the reader is referred to the web version of this article.

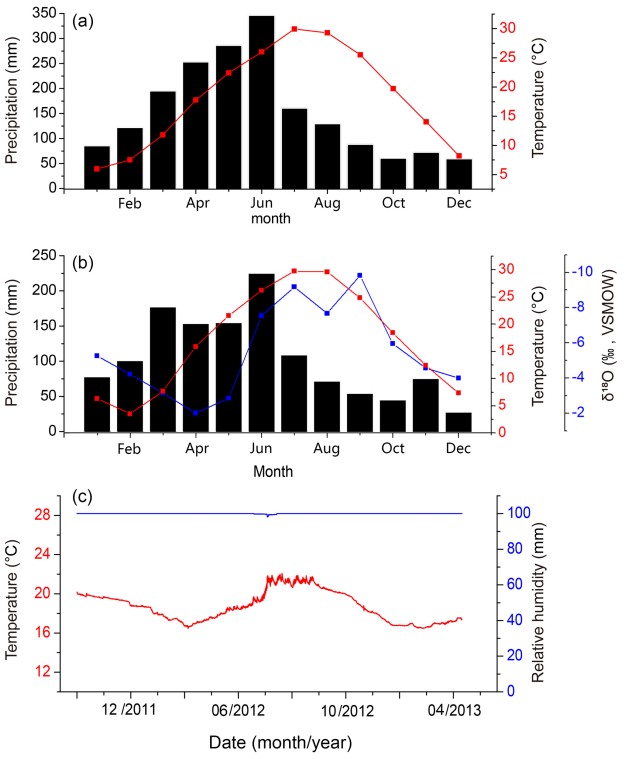

Figure 2. Mean monthly temperature, precipitation and $\delta^{18}O$ value from two meteorological stations close to the study area and environmental monitoring in Shennong Cave. **(a)** Mean monthly air temperature (red line) and precipitation (black column) from the Guixi meteorological station for 1951–2010. **(b)** Mean monthly air temperature (red line), precipitation (black column) and $\delta^{18}O$ value (blue line) from the Changsha GNIP station for 1988–1992. **(c)** Air temperature (red line) and relative humidity (blue line) in Shennong Cave from October 2011 to April 2013.

in continental China at about 4.2 ka BP (Yao and Thompson, 1992; Jin and Liu, 2002; Zhou et al., 2002; Zhong et al., 2017; Xu et al., 2006; Yao et al., 2017), but changes in the spatial distribution of precipitation are also discussed (Tan et al., 2008, 2018a, b; Huang et al., 2010, 2011; Wu et al., 2017). For example, a grain-size record from Daihai Lake, north China, suggests a decrease in monsoon precipitation between 4.4 and 3.1 ka BP with a very dry interval between 4.4 and 4.2 ka BP (Peng et al., 2005). Extreme flooding during the 4.2 ka BP event was identified by paleoflood deposits in the middle reaches of the Yellow River (Huang et al., 2010, 2011). Wu et al. (2017) reported evidence of two extraordinary paleoflood events in the middle reaches of the Yangtze River at 4.9–4.6 and 4.1–3.8 ka BP, closely related to the expansion of the Jianghan lakes. These extreme hydroclimate events may have accelerated the collapse of the Shijiahe culture in the middle reaches of the Yangtze River (Wu et al., 2017). Multiple proxies in four stalagmites from Xianglong Cave, south of the Qinling Mountains, indicate that the upper Hanjiang River region experienced a wet climate during the 4.2 ka BP event (Tan et al., 2018a). Peat records provide a broad picture of climate variations in southeast China (SEC) during the Holocene (Zhou et al., 2004; Zhong et al., 2010a, b, c, 2015, 2017). The resolution of these records, however, is not high enough to study the detailed structure of the 4.2 ka BP event. So far, there has only been one published stalagmite record from SEC (Xiangshui Cave; Fig. 1), indicating a wet interval during the 4.2 ka BP event (Zhang et al., 2004).

The aim of this work was to obtain a high-resolution stalagmite-based record from SEC to study the hydroclimatic variations during the 4.2 ka BP event and to compare them to records in northern China in order to explore the possible north–south precipitation gradient during this event.

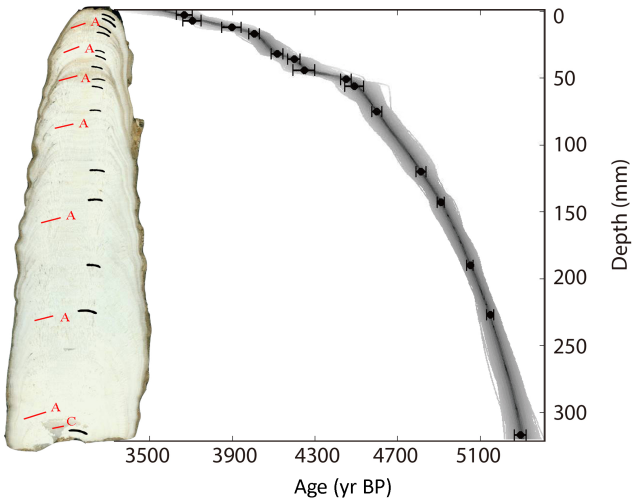

Figure 3. Polished section (left) and age model (right) of stalagmite SN17. Sampling positions for XRD analyses (red lines; A aragonite, C calcite) and ^{230}Th datings (black lines) are shown on the slab. SN17 age model and modeled age uncertainties using COPRA; error bars on ^{230}Th dates indicate 2σ analytical errors. The gray band depicts the 95 % confidence interval.

2 Study area and sample

Shennong Cave (28°42′ N, 117°15′ E; 383 m a.s.l.) is located in the northeastern Jiangxi Province, SEC (Fig. 1), a mid-subtropical region strongly influenced by the East Asian summer monsoon (EASM). Mean annual precipitation and temperature at the nearest meteorological station (Guixi station; 1951–2010 CE) are 1857 mm and 18.5 °C, respectively (Fig. 2a). Shennong Cave is located in a region of spring persistent rain. The rainy season includes both summertime monsoon rainfall and spring persistent rain (Tian and Yasunari, 1998; Wan et al., 2008; Zhang et al., 2018). The latter is a unique synoptic and climatic phenomenon that occurs from March until mid-May, mostly south of the Yangtze River (about 24 to 30° N, 110 to 120° E; Tian and Yasunari, 1998; Wan and Wu, 2007, 2009). EASM precipitation lasts from mid-May to September (Wang and Lin, 2002). In the region of spring persistent rain, the EASM (May to September) precipitation accounts for 54 % of the annual precipitation and the non-summer monsoon (NSM, October to next April) precipitation accounts for 46 % (Zhang et al., 2018). The distribution of the EASM vs. NSM precipitation amount in this region is distinctly different from that in the northern and southwestern part of monsoonal China, where the mean annual percentage of EASM (65 %–90 %) is much higher than the mean annual percentage of NSM (10 %–35 %). Data from the nearest GNIP station in Changsha, also located in the region of spring persistent rain, indicate that the δ^{18}O values of EASM precipitation are lower compared with those of NSM precipitation (Fig. 2b). A full 2 years of monitoring data (2011–2013) in Shennong Cave indicate that the speleothem δ^{18}O values reflected drip water δ^{18}O values inherited from the amount-weighted annual precipitation δ^{18}O outside the cave. Therefore, different from the southwestern and northern part of monsoonal China where the speleothem δ^{18}O values are mainly influenced by EASM precipitation, speleothem δ^{18}O from Shennong Cave is controlled by both EASM and NSM precipitation (Zhang et al., 2018).

The cave developed in the carboniferous limestone of the Chuan-shan and Huang-long groups, which are mainly composed of limestone and interbedded dolostone. The thickness of the cave roof ranges from about 20 to about 80 m, with an average of ∼ 50 m. The overlying vegetation consists mainly of secondary forest tree species such as *Pinus*, *Cunninghamia* and *Phyllostachys*, and shrub-like *Camellia oleifera* and *Ilex*, which are C_3 plants (Zhang et al., 2015). A full 2 years of monitoring data show that the mean temperature in the cave is 19.1 °C with a standard deviation of 2.5 °C (Fig. 2c), consistent with mean annual air temperature outside the cave (Fig. 2a). The relative humidity in the interior of the cave approaches 100 % during most of the year (Fig. 2c). Abundant aragonite and calcite speleothems are present in the cave. Their mineralogy is likely controlled by the Mg/Ca ratio of the drip water, reflecting the variable dolomite content of the host rock (De Choudens-Sanchez and Gonzalez, 2009; Zhang et al., 2014, 2015). All aragonite stalagmites were deposited within ∼ 1.5 km of the cave entrance where the bedrock is dolomite, and all calcite stalagmites were deposited in more distal parts of the cave where limestone constitutes the host rock (Zhang et al., 2015).

In November 2009 stalagmite SN17 (Fig. 3), 320 mm in length, was collected 200 m behind the cave entrance where the bedrock is dolomite. X-ray diffraction (XRD) analyses suggest that the stalagmite is composed of aragonite, except for the bottom section below 318 mm, which is composed of calcite (Fig. 3). The calcite section was not included in the present study.

3 Methods

3.1 ^{230}Th dating

A total of 15 subsamples for ^{230}Th dating were drilled along the growth axis of SN17 (Fig. 3) with a handheld carbide dental drill, and were dated on a multi-collector inductively coupled plasma mass spectrometer (MC-ICP-MS, Neptune Plus) at the Department of Earth Sciences, University of Minnesota, and the Institute of Global Environmental Change, Xi'an Jiaotong University (Cheng et al., 2000, 2013). The chemical procedures used to separate uranium and thorium followed those described by Edwards et al. (1987).

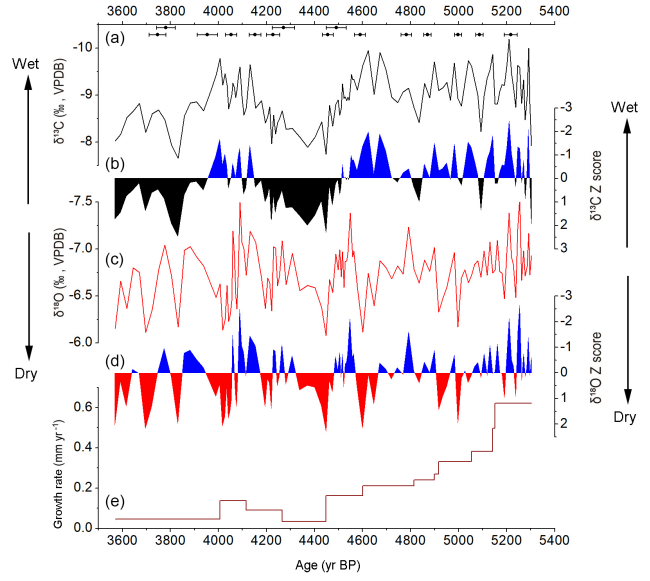

Figure 4. The δ^{13}C **(a)** and δ^{18}O **(c)** records and growth rate **(e)** of stalagmite SN17. The δ^{13}C and δ^{18}O records were normalized to standard records of z-scored δ^{13}C **(b)** and z-scored δ^{18}O **(d)** for comparison, respectively. ^{230}Th dates and error bars are shown on the top of panel **(a)**.

3.2 Stable isotope analyses

A total of 120 subsamples for stable isotope analyses were drilled along the central axis of SN17 at intervals of 1 mm between 0 and 70 and 5 mm between 70 and 320 mm of distance from the top. The samples were analyzed using a gas-source stable isotope ratio mass spectrometer (Isoprime100) equipped with a MultiPrep system at the Institute of Earth Environment, Chinese Academy of Sciences (IEECAS). The international standard NBS19 and the laboratory standard HN were analyzed after every 10 subsamples to monitor data reproducibility. All oxygen and carbon isotope compositions are reported in per mil relative to the Vienna Pee Dee Belemnite (VPDB). Reproducibility of δ^{18}O and δ^{13}C values was better than 0.1 ‰ and 0.08 ‰ (2σ), respectively.

4 Results

4.1 Chronology

The ^{230}Th dates are all in stratigraphic order and no significant hiatus was observed (Table 1 and Fig. 3). Because of the high uranium concentrations (1120–6380 ppb) and relatively low thorium concentrations (56–195 ppt), most of the dating errors are less than 6 ‰. We used COPRA (Breitenbach et al., 2012) to establish an age model of stalagmite SN17, which grew from 3570 to 5303 yr BP (Fig. 3).

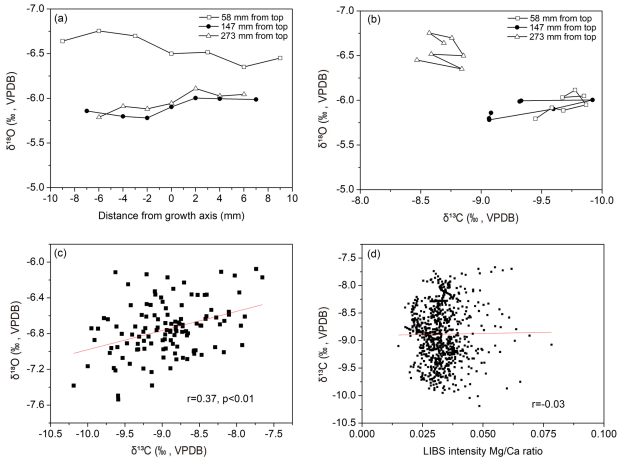

Figure 5. Hendy tests of stalagmite SN17 (coeval δ^{18}O data in panel **a** and δ^{18}O versus δ^{13}C in panel **b**); correlation between δ^{13}C and δ^{18}O values **(c)** and between δ^{13}C values and Mg/Ca ratios **(d)** measured along the stalagmite growth axis.

4.2 δ^{13}C and δ^{18}O records

The temporal resolution of the δ^{13}C and δ^{18}O records ranges from 6 to 21 years. The δ^{13}C values fluctuate around −9.18 ‰ (mean value) during the period 5.3 to 4.5 ka BP and increase to −8.69 ‰ between 4.5 and 3.57 ka BP (Fig. 4a). δ^{18}O fluctuates around −6.75 ‰ (mean value) during the period 5.3 to 3.57 ka BP on decadal to centennial timescales (Fig. 4c). The δ^{18}O record is broadly similar to the δ^{13}C record between 5.3 and 3.57 ka BP (Figs. 4 and 6c), with a significantly positive correlation ($r = 0.37$, $p<0.01$; Fig. 5c). Both δ^{13}C and δ^{18}O records were normalized to the standard z score (Figs. 4b and d), which clearly shows the decadal to centennial variability during the interval of 5.3–3.57 ka BP. Z-scored δ^{13}C values are above 0 during the intervals of 5.3–4.5 and 4.15–3.95 ka BP and below 0 during the intervals of 4.5–4.15 and 3.95–3.57 ka BP on centennial timescales (Fig. 4b). Z-scored δ^{18}O records are above 0 during the intervals of 5.3–5.05, 4.9–4.66, 4.57–4.48 and 4.32–4.06 and below 0 during the intervals of 5.05–4.9, 4.66–4.57, 4.48–4.32 and 4.06–3.57 ka BP on centennial timescales (Fig. 4d). The growth rate of SN17 shows a persistently decreasing trend from 0.62 to 0.034 mm yr^{-1} between 5.3 and 4.5 ka BP, followed by low values during the period 4.5 to 3.57 ka BP with relatively higher values between 4.26 and 4.0 ka BP (Fig. 4e). The periods of higher growth rate correspond to the periods of lower δ^{18}O and δ^{13}C values, which we infer to be the time of more summer monsoon precipitation (see below).

Table 1. ^{230}Th results of stalagmite SN17 from Shennong Cave. The errors are 2σ.

Distance from the top (mm)	Sample number	^{238}U (ppb)	^{232}Th (ppt)	^{230}Th/^{232}Th (atomic $\times 10^{-6}$)	δ^{234}U* (measured)	^{230}Th/^{238}U (activity)	^{230}Th age (yr) (uncorrected)	^{230}Th age (yr BP)*** (corrected)	$\delta^{234}U^{**}_{initial}$ (corrected)
3	SN17-3	2063 ± 1.9	1025 ± 22	1388 ± 33	235.5 ± 1.4	0.0418 ± 0.0004	3736 ± 38	3668 ± 38	238 ± 1
7	SN17-7	1146 ± 1.6	2511 ± 51	320 ± 7	235.3 ± 2.1	0.0426 ± 0.0003	3820 ± 24	3707 ± 43	238 ± 2
12	SN17-12	1757 ± 1.8	984 ± 22	1302 ± 33	233.6 ± 1.5	0.0442 ± 0.0005	3979 ± 46	3897 ± 47	236 ± 2
17	SN17-17	2617 ± 5.7	132 ± 10	14960 ± 1115	243.2 ± 2.4	0.0457 ± 0.0003	4076 ± 26	4007 ± 26	246 ± 2
32	SN17-32	2535 ± 4.9	195 ± 11	10103 ± 565	252.1 ± 2.2	0.0472 ± 0.0003	4187 ± 27	4117 ± 27	255 ± 2
36	SN17-36	3572 ± 4.9	1814 ± 39	1560 ± 35	247.1 ± 1.7	0.0481 ± 0.0003	4279 ± 29	4268 ± 30	250 ± 2
44	SN17-44	1122 ± 1.2	151 ± 10	6034 ± 420	265.5 ± 1.9	0.0492 ± 0.0006	4319 ± 52	4248 ± 52	269 ± 2
51	SN17-51	1035 ± 1.7	1169 ± 24	763 ± 16	279.4 ± 1.9	0.0522 ± 0.0002	4540 ± 18	4452 ± 25	283 ± 2
56	SN17-56	2976 ± 3.6	82 ± 20	31024 ± 7484	264.4 ± 1.4	0.0519 ± 0.0005	4560 ± 18	4491 ± 46	268 ± 1
75	SN17-75	4619 ± 7.3	66 ± 14	61740 ± 12772	268.8 ± 1.9	0.0532 ± 0.0003	4668 ± 25	4600 ± 25	272 ± 2
120	SN17-120	4640 ± 8.5	225 ± 14	19262 ± 1186	290.3 ± 2.2	0.0566 ± 0.0003	4883 ± 24	4814 ± 24	294 ± 2
143	SN17-143	2993 ± 5.2	1031 ± 21	2810 ± 58	312.9 ± 2.2	0.0587 ± 0.0002	4980 ± 17	4910 ± 17	317 ± 2
190	SN17-190	6380 ± 9.5	56 ± 10	114548 ± 20151	322.2 ± 1.4	0.0608 ± 0.0002	5120 ± 16	5052 ± 16	327 ± 1
227	SN17-227	4436 ± 10.2	873 ± 18	5189 ± 106	323.7 ± 2.2	0.0619 ± 0.0002	5216 ± 17	5149 ± 17	329 ± 2
317	SN17-317	6886 ± 31.0	2221 ± 45	3273 ± 67	331.7 ± 3.0	0.0640 ± 0.0003	5363 ± 29	5294 ± 29	337 ± 3

U decay constants: $\lambda_{238} = 1.55125 \times 10^{-10}$ and $\lambda_{234} = 2.82206 \times 10^{-6}$. Th decay constant: $\lambda_{230} = 9.1705 \times 10^{-6}$ (ref. 56). * $\delta^{234}U = ([^{234}U/^{238}U]_{activity} - 1) \times 1000$. ** $\delta^{234}U_{initial}$ was calculated based on ^{230}Th age (T), i.e., $\delta^{234}U_{initial} = \delta^{234}U_{measured} \times e^{\lambda 234 \times T}$. Corrected ^{230}Th ages assume the initial ^{230}Th/^{232}Th atomic ratio of $4.4 \pm 2.2 \times 10^{-6}$. Those are the values for a material at secular equilibrium, with the bulk earth ^{232}Th/^{238}U value of 3.8. BP stands for "before present", and the "present" is defined as the year 1950 CE.

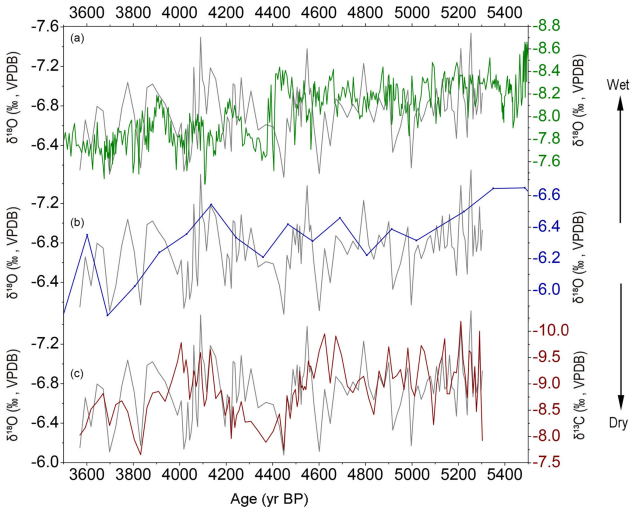

Figure 6. Replication of the $\delta^{18}O$ records from three caves (Shennong Cave: gray lines, Dongge Cave: green line, Xiangshui Cave: dark blue line) during the overlapping growth period and comparison between $\delta^{18}O$ (gray line) and $\delta^{13}C$ (brown line) records of SN17 (C).

5 Discussion

5.1 Test of equilibrium deposition

Speleothem $\delta^{18}O$ can be used to indicate climatic variation provided that the speleothem was precipitated at or close to isotopic equilibrium. The "Hendy test" is a widely used approach to explore to what extent calcite deposition on the stalagmite surface occurred in isotopic equilibrium with the parent drip water. Following Hendy (1971), 21 subsamples from three growth layers were analyzed; no progressive increase in $\delta^{18}O$ along individual growth layers and no significant correlation of coeval $\delta^{18}O$ and $\delta^{13}C$ values were found (Fig. 5a and b). This suggests (but does not prove) that the stalagmite SN17 was deposited close to isotopic equilibrium. On the other hand, $\delta^{18}O$ and $\delta^{13}C$ values show a statistically significant covariance along the growth axis ($r = 0.37$, $p<0.01$; Fig. 5c), suggesting that the speleothem might be effected by kinetic fractionation (Dorale and Liu, 2009). Some studies, however, demonstrated that stalagmites showing a significant correlation between $\delta^{18}O$ and $\delta^{13}C$ can also have formed under isotopic equilibrium if both parameters are controlled by the common factors (Dorale et al., 1998; Dorale and Liu, 2009; Tan et al., 2018a). A more robust test is the replication of $\delta^{18}O$ records from different caves (Dorale et al., 1998; Wang et al., 2001; Dorale and Liu, 2009; Cai et al., 2010). The $\delta^{18}O$ records of SN17 and those from Dongge (Wang et al., 2005) and Xiangshui Cave (Zhang et al., 2004), located southwest of Shennong Cave (Fig. 1), show remarkable similarities in the overlapping interval (Fig. 6a and b). The replication of these records further confirms that aragonite in stalagmite SN17 was most likely deposited close to isotopic equilibrium; i.e., its $\delta^{18}O$ variations primarily reflect climatic changes.

5.2 Interpretation of $\delta^{18}O$ and $\delta^{13}C$

The climatic significance of the speleothem $\delta^{18}O$ from monsoonal China has been intensively debated in recent years. Most scientists agree that speleothem $\delta^{18}O$ in monsoonal China represent variations in EASM intensity and/or changes in spatially integrated precipitation between different moisture sources and the cave site on millennial timescales (Cheng et al., 2016). Some researchers, however, suggest that the Chinese speleothem $\delta^{18}O$ is influenced by moisture circulation on interannual to centennial timescales (Tan, 2009, 2014, 2016). In the region of spring persistent rain, the speleothem $\delta^{18}O$ values from Shennong Cave are controlled by both EASM and NSM precipitation. A 200-year speleothem $\delta^{18}O$ record from E'mei Cave, located 160 km northwest of Shennong Cave, shows a significantly negative correlation with both the EASM precipitation amount ($r = -0.54$, $p<0.01$) and the EASM / NSM ratio ($r = -0.67$, $p<0.01$) during 1951–2009 CE (Fig. 3 in Zhang et al., 2018). The EASM precipitation amount varies in the same direction as the EASM / NSM ratio; i.e., an increasing (decreasing) EASM / NSM ratio corresponds to more (less) EASM precipitation. In addition, the E'mei $\delta^{18}O$ record also exhibits a coherent variation with the drought–flood index during 1810–2010 CE on decadal to centennial timescales (Fig. 2 in Zhang et al., 2018). This indicates that E'mei $\delta^{18}O$ is likely dominated by the EASM precipitation amount on decadal to centennial timescales. Therefore, we suggest that the stalagmite $\delta^{18}O$ record from Shennong Cave, similar to E'mei Cave, might be primarily influenced by the EASM / NSM ratio, is also affected by the EASM precipitation amount on interannual to decadal timescales, and can be dominated by the EASM precipitation amount on decadal to centennial timescales, i.e., lower (higher) $\delta^{18}O$ values corresponding to higher (lower) EASM / NSM ratios and more (less) EASM precipitation.

Changes in speleothem $\delta^{13}C$ are generally controlled by vegetation density and composition in the catchment, which vary according to the hydroclimate (Genty et al., 2001, 2003, 2006; McDermott, 2004; Baldini et al., 2005; Cruz Jr. et al., 2006; Fairchild et al., 2006; Fleitmann et al., 2009; Noronha et al., 2015; Wong and Breeker, 2015). In regions where the vegetation type is predominantly C_3 or C_4 plants, a dry climate will lead to a reduction of the vegetation cover, density and soil microbial activity as well as an increase in the groundwater residence time, allowing more $\delta^{13}C$-enriched bedrock to be dissolved. In addition, prior calcite precipitation (PCP) in the vadose zone will result in higher $\delta^{13}C$ values accompanied by increased Mg/Ca ratios in speleothems (Baker et al., 1997). Slow drip rates and increased evaporation and/or ventilation inside the cave will lead to higher $\delta^{13}C$ values, usually accompanied by kinetic isotopic frac-

tionation (Fairchild et al., 2000; Oster et al., 2010; Frisia et al., 2011; Li et al., 2011; Tremaine et al., 2011; Meyer et al., 2014). In Jiangxi Province, a region presently occupied by mostly C_3 plants, no evidence has been found for a replacement of C_3 plants by C_4 plants during the middle to late Holocene (Zhou et al., 2004; Zhong et al., 2010b). There is no significantly positive correlation between $\delta^{13}C$ values and Mg/Ca ratios between 5.3 and 3.57 ka BP (Fig. 5d). In Shennong Cave ventilation is weak and relative humidity remains close to 100 % throughout the year. Rapid CO_2 degassing is less common under these conditions. Stalagmite SN17 was likely deposited close to isotopic equilibrium, as confirmed by the Hendy test and the "replication test" (Sect. 5.1). The $\delta^{13}C$ variations in this stalagmite were primarily driven by vegetation density and soil bioproductivity associated with hydroclimatic variations but not by PCP or rapid CO_2 degassing, with lower $\delta^{13}C$ values corresponding to a denser vegetation cover associated with a wet climate and vice versa (Zhang et al., 2015).

5.3 Hydroclimate between 5.3 and 3.57 ka BP

Previous speleothem studies from monsoonal China suggested a coherent trend of decreasing precipitation from the early to the late Holocene (Wang et al., 2005; Hu et al., 2008; Cai et al., 2010, 2012; Dong et al., 2010, 2015; Jiang et al., 2013; Tan et al., 2018a), which follows the gradually decreasing Northern Hemisphere summer insolation. Our $\delta^{13}C$ record exhibits a similarly increasing trend (Fig. 4a, b), indicating that the climate in our study area changed from wetter to drier conditions between 5.3 and 3.57 ka BP. Although the growth rate of stalagmites is often not a direct function of precipitation amount (Railsback, 2018), some studies suggest that in monsoonal China changes in the growth rate of stalagmite can be influenced by variations in monsoon precipitation (Wang et al., 2005). The long-term decreasing trend in growth rate, broadly consistent with changes in the $\delta^{13}C$ record, is possible related to decreased monsoon precipitation between 5.3 and 3.57 ka BP (Fig. 4). But it should be noted that more monitoring data are needed to confirm this relationship between growth rate and precipitation in our study cave. The long-term trend in $\delta^{18}O$ is less significant than those of $\delta^{13}C$ and growth rate (Fig. 4) and might be caused by changes in precipitation seasonality since the mid-Holocene, i.e., variations in the EASM / NSM ratio. In this paper, we focus on the timing and nature of the 4.2 ka BP event. The long-term trend of $\delta^{18}O$ is not discussed in detail because it remains unclear how EASM and NSM precipitation varied during the Holocene.

As discussed in Sect. 5.2, the SN17 $\delta^{18}O$ might be dominated by the EASM precipitation amount on decadal to centennial timescales, although the EASM / NSM ratio has a significant impact on interannual to decadal timescales. On decadal to centennial timescales the SN17 $\delta^{18}O$ record shows a coherent variability with the $\delta^{13}C$ record (Fig. 6c), which is primarily influenced by the EASM precipitation amount but not by seasonal precipitation $\delta^{18}O$. In addition, the SN17 $\delta^{18}O$ record is remarkably similar to the $\delta^{18}O$ record from Dongge Cave (Fig. 6a), which is dominated by summer monsoon precipitation (Wang et al., 2005). These observations indicate that, on decadal to centennial timescales, variations in SN17 $\delta^{18}O$ might primarily reflect changes in the EASM precipitation amount, although the EASM / NSM ratio may also have an impact, with higher (lower) $\delta^{18}O$ values corresponding to decreased (increased) summer monsoon precipitation. The asynchronous variations between $\delta^{13}C$ and $\delta^{18}O$ during the short intervals of 4.7–4.6, 4.3–4.2 and 4.05–3.95 ka BP (Fig. 6c) may be ascribed to the delayed response of vegetation density to variations in the EASM precipitation amount or the EASM / NSM ratio. During 4.5–3.57 ka BP, a wet interval between 4.2 and 3.9 ka BP can be identified in both $\delta^{18}O$ and $\delta^{13}C$ records, consistent with the time of high growth rate between 4.26 and 4.0 ka BP (Figs. 4 and 6c).

Therefore, we suggest that the climate in the study area between 5.3 and 4.5 ka BP was dominantly wet and changed to a rather dry climate between 4.5 and 3.57 ka BP, interrupted by one wet interval between 4.2 and 3.9 ka BP (Figs. 4 and 6c). It indicates that the climate in our study area during the 4.2 ka BP event (4.2–3.9 ka BP) was predominantly wet.

5.4 Comparison with other records in monsoonal China covering the 4.2 ka BP event

The nature and timing of the 4.2 ka BP event in southern and northern China are still controversial because the discrepancies might also be caused by the large dating uncertainties and the low proxy resolution in some records. By reviewing records from the monsoon region of China, Tan et al. (2018a) have already proposed a "north dry, south wet" pattern during the 4.2 ka BP event; however, more speleothem records from SEC are still needed to confirm this pattern. In this section, we compare high-precision and high-resolution speleothem records from monsoonal China during the interval of 5.4–3.6 ka BP.

For northern and southwestern China, the stalagmite $\delta^{18}O$ record from Lianhua Cave (Fig. 1) shows a long-term decreasing trend of summer monsoon precipitation (Fig. 7a; Dong et al., 2015), consistent with both $\delta^{18}O$ and $\delta^{13}C$ records of stalagmites from Nuanhe Cave in northeastern China (Fig. 1; Tan and Cai, 2005; Wu et al., 2011; Zhang and Wu, 2012). These records indicate that the climate in northern China gradually varied from wet to dry between 5.4 and 3.6 ka BP, and the climate was very dry during the interval of 4.2–3.9 ka BP. The $\delta^{18}O$ record from Dongge Cave, southwest of monsoonal China, reveals a dry event between 4.4 and 3.95 ka BP (Fig. 7g; Wang et al., 2005), which is consistent with decreased precipitation from the Indian summer monsoon during the interval of 4.3–3.9 ka BP (Fig. 7h; Berkelhammer et al., 2012), and dry intervals in the stalagmite records from Shigao, Dark and Xianren Cave, south-

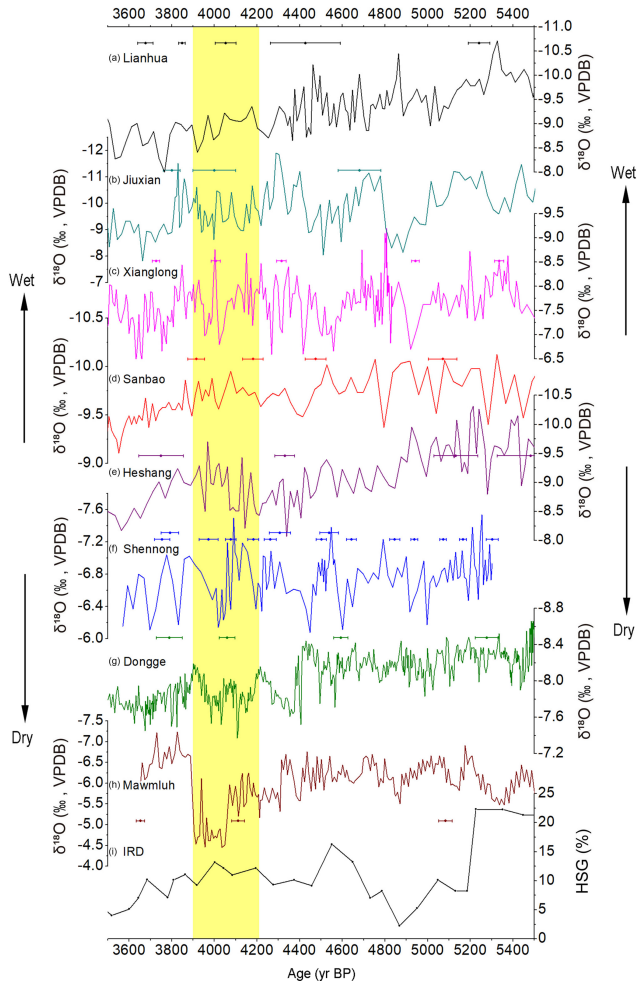

Figure 7. Comparison of $\delta^{18}O$ records from **(a)** Lianhua Cave (Dong et al., 2015), **(b)** Jiuxian Cave (Cai et al., 2010), **(c)** Xianglong Cave (Tan et al., 2018a), **(d)** Sanbao Cave (Dong et al., 2010), **(e)** Heshang Cave (Hu et al., 2008), **(f)** Shennong Cave (this study), **(g)** Dongge Cave (Wang et al., 2005), **(h)** Mawmluh Cave (Berkelhammer et al., 2012) and the ice-rafted hematite-stained grain (HSG) record from the North Atlantic (Bond et al., 2001). ^{230}Th dates and error bars are illustrated with different colors for each stalagmite. The yellow bar marks the dry interval in northern and southwestern China and the wet interval in central and southeastern China during the 4.2 ka BP event (4.2–3.9 ka BP).

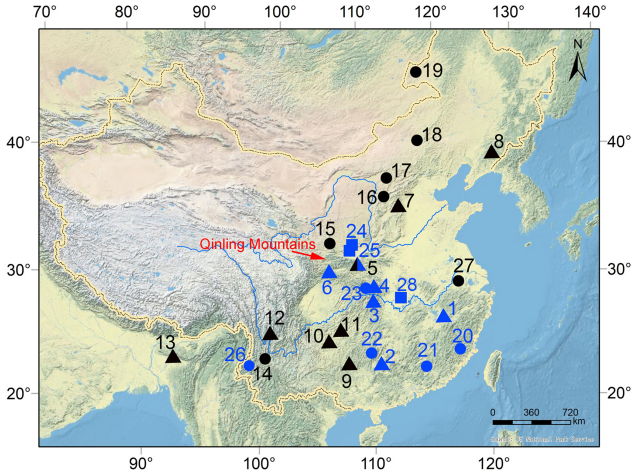

Figure 8. Map showing some locations discussed in the text. 1: Shennong Cave, this study; 2: Xiangshui Cave (Zhang et al., 2004); 3: Heshang Cave (Hu et al., 2008); 4: Sanbao Cave (Dong et al., 2010); 5: Jiuxian Cave (Cai et al., 2010), 6: Xianglong Cave (Tan et al., 2018a); 7: Lianhua Cave (Dong et al., 2015); 8: Nuanhe Cave (Tan, 2005); 9: Dongge Cave (Wang et al., 2005); 10: Dark Cave (Jiang et al., 2013); 11: Shigao Cave (Jiang et al., 2012); 12: Xianren Cave (Zhang et al., 2006); 13: Mawmluh Cave (Berkelhammer et al., 2012); 14: Erhai Lake (Zhou et al., 2003); 15: Tianchi Lake (Zhao et al., 2010); 16: Gonghai Lake (Chen et al., 2015); 17: Daihai Lake (Xiao et al., 2018a); 18: Dali Lake (Xiao et al., 2008); 19: Hulun Lake (Xiao et al., 2018b); 20: Daiyunshan peat (Zhao et al., 2017), 21: Dahu peat (Zhou et al., 2004), 22: Daping peat (Zhong et al., 2010a); 23: Dajiuhu peat (Ma et al., 2008); 24: Chengjiachuan site (Huang et al., 2010); 25: Huxizhuang loess–soil profile (Huang et al., 2011); 26: Tengchongqinghai Lake (Zhang et al., 2017); 27: Gaochun profile (Yao et al., 2017); 28: Zhongqiao site (Wu et al., 2017). The solid triangle, dot and square denote stalagmite records, lake sediment–peat records and paleoflood sediment records, respectively. Black and blue indicate a dry and a wet climate during the 4.2 ka BP event, respectively. The base map is the same as that in Fig. 1.

western China (Fig. 8 and references therein); however, a wet climate is documented by multi-proxy data from a maar lake in southwest China (Fig. 8; Zhang et al., 2017). The prominent drought during the 4.2 ka BP event was also recorded by various other archives from sites in northern and southwestern China (Fig. 8 and references therein).

For north and south of the Qinling Mountains, two stalagmite $\delta^{18}O$ records from Jiuxian and Xianglong Cave south of the mountains exhibit coherent variations on centennial timescales but neither of them shows a long-term increasing trend (Fig. 7b and c; Cai et al., 2010; Tan et al., 2018a). Both $\delta^{18}O$ records reveal increased monsoon precipitation between 4.3 and 3.8 ka BP, indicating that the climate south of the Qinling Mountains was wet during the 4.2 ka BP event (Tan et al., 2018a). It should be noted that there is an asynchronous variation during the interval of 4.2–3.9 ka BP between the Jiuxian and Xianglong $\delta^{18}O$ records, which might be due to either dating uncertainties in the Jiuxian record or the spatial distribution of monsoon precipitation between these two regions. The extraordinary flood during the 4.2 ka BP event was also identified in the middle reaches of the Yellow River north of the Qinling Mountains, north-central China (Fig. 8; Huang et al., 2010, 2011).

For south-central China, two stalagmite $\delta^{18}O$ records from Sanbao (Fig. 7d; Dong et al., 2010) and Heshang (Fig. 7e; Hu et al., 2008) Cave in the middle reaches of the Yangtze River, south-central China, also indicate a wet interval between 4.2 and 3.9 ka BP, which is consistent with a $\delta^{13}C$ peat record

from the Dajiuhu basin (Ma et al., 2008) and paleoflood sediments from Jianghan Plain (Wu et al., 2017) in the same region (Fig. 8). δ^{15}N and δ^{13}C records from the Daping swamp in Hunan Province, south-central China, also reveal a wet interval at 4.5–4.0 ka BP (Fig. 8; Zhong et al., 2017).

For SEC, SN17 δ^{18}O and δ^{13}C records reveal a wet interval between 4.2 and 3.9 ka BP on centennial timescales (Figs. 6c and 7f), which is consistent with the speleothem δ^{18}O record from Xiangshui Cave (Fig. 6b). A record of total organic carbon (TOC) from the Dahu swamp, Jiangxi Province, located 450 km south of Shennong Cave, indicates a dry climate between 6.0 and 4.0 ka BP, with a short-lived wet event at 4.1 ka BP (Fig. 8; Zhou et al., 2004). Subsequent multi-proxy records of several new cores from this site also revealed a prevailingly dry climate between 6.0 and 3.0 ka BP with a wet interval at 4.2–3.9 ka BP (Zhong et al., 2010a, b, c). Pollen data from two sediment profiles from Daiyunshan, a mountain in SEC, indicate a centennial-scale wet event at 4.4 ka BP (Fig. 8; Zhao et al., 2017). These published records from SEC are consistent with the SN17 δ^{18}O and δ^{13}C records within error, indicating a wet climate in SEC during the 4.2 ka BP event (Fig. 8).

To sum up, high-resolution stalagmite records indicate that the climate during the 4.2 ka BP event was dry in northern and southwestern China and wet in southern China (Figs. 7 and 8), and the nature and timing of this event were different in different regions of monsoonal China. The remarkable dry climate lasted from ∼ 4.4 to 3.9 ka BP in northern and southwestern China (Fig. 8). South-central China and SEC were dry between 4.4 and 4.2 ka BP and wet between 4.2 and 3.9 ka BP (Fig. 8). The climate was wet between 4.4 and 4.2 ka BP but was dry between 4.2 and 3.9 ka BP at Jiuxian Cave (Figs. 7b and 8), southeast of the Qinling Mountains, and the climate was wet between 4.3 and 3.8 ka BP at Xianglong Cave, southwest of this mountain range (Figs. 7c and 8). A dry and cold period during the 4.2 ka BP event was identified in a sediment profile from Gaochun, west of Taihu Lake, eastern China (Fig. 8, Yao et al., 2017). Therefore, we suggest that the boundary between the dry north and the wet south during the 4.2 ka BP event was probably located along the northern rim of the Qinling Mountains and the lower reaches of the Yangtze River (Fig. 8).

This south–north distribution of monsoon precipitation might have been caused by a weakened EASM intensity, which could have resulted from a reduced Atlantic Meridional Overturning Circulation (AMOC) recorded by higher abundances of ice-rafted debris (IRD) in the North Atlantic (Fig. 7i). Strong freshwater input into the North Atlantic derived from melting icebergs periodically reduced the AMOC (Bond et al., 2001), causing a temperature decrease in the high northern latitudes and intensified midlatitude westerlies. As a consequence, the Intertropical Convergence Zone and Northern Hemisphere westerly jet got stronger, migrated southward, and weakened the Indian summer monsoon and the EASM (Wang et al., 2001; Chiang et al., 2015). The stronger westerly jet and the weakened EASM delayed the westerly jet transition from south of the Tibetan Plateau to the north in early to middle May and postponed the onset of the EASM (Chiang et al., 2015; Tan et al., 2018a). The rain belt migrated southward and remained longer in southern China than normal, which reduced rainfall in northern and southwestern China (Fig. 7a and g) but enhanced rainfall in central and southern China (Fig. 7c, d, e and f) during the periods of 4.7–4.5 and 4.2–3.9 ka BP.

The SN17 δ^{18}O record exhibits a coherent variation with the δ^{18}O record from Dongge Cave within error on centennial timescales but there are some differences in amplitude (Figs. 6a and 7), which can also be found between the Jiuxian and Xianglong records and between the Sanbao and Heshang records (Fig. 7). These discrepancies might be due to chronology offsets because some records are constrained by two to three dates only. Alternatively, the different amplitudes of these records might be caused by the spatial distribution of monsoon precipitation, reflecting the position and residence time of the rain belt associated with variations in EASM intensity. For example, during the period of 4.2–3.9 ka BP, reduced AMOC caused a dry climate in northern and north-central China but a wet climate in south-central China and SEC (Figs. 7 and 8). During the period of 4.6–4.5 ka BP, however, the records show a dry climate from northern China to south-central China but a wet climate in SEC (Figs. 7 and 8). Because the AMOC was in a very weak stage at 4.55 ka BP this could have resulted in a weakened EASM and a further southward shift of the monsoonal rain belt, possibly causing a dry climate in south-central China and a wet climate in SEC. Recently, Yan et al. (2018) used a set of long-term climate simulations and suggested that the 4.2 ka BP event could be related to the slowdown of the AMOC but was more likely caused by internal variability in the climate system. Detailed modeling studies and additional high-resolution records are needed to further investigate the possible causes and mechanisms of this event.

6 Conclusions

We reconstructed monsoon precipitation variations in the lower Yangtze River region, SEC, between 5.3 and 3.57 ka BP based on δ^{18}O and δ^{13}C records of a precisely dated, high-resolution stalagmite from Shennong Cave in the northern part of Jiangxi Province. The long-term trend of increasing δ^{18}O and δ^{13}C values together with a decreasing growth rate is consistent with other stalagmite and peat records from monsoonal China, showing increased monsoon rainfall between 5.3 and 4.5 ka BP and decreased monsoon rainfall between 4.5 and 3.6 ka BP in the study area. A wet episode at 4.2–3.9 ka BP is in agreement with other records from southern China. The boundary between a dry climate in northern China and a coeval wet climate in southern China during the 4.2 ka BP event was probably located to

the north of the Qinling Mountains and the lower reaches of the Yangtze River. This north–south distribution of monsoon precipitation may have been caused by a weakened summer monsoon, which itself may have been related to a reduced AMOC. During a weak summer monsoon, the rain belt remains longer in its southern position, resulting in reduced precipitation in northern China and enhanced precipitation in southern China.

Data availability. Research data from this study are available on request (zhanghaiwei@xjtu.edu.cn).

Author contributions. HZ designed the research and wrote the first draft of the paper. HC, YC, CS and AS revised the paper. HZ and YC did the fieldwork and collected the samples. HZ, YC and LT conducted the oxygen isotope measurements. HZ, HC, GK and RLE conducted the ^{230}Th dating. All authors discussed the results and provided input on the paper.

Competing interests. The authors declare that they have no conflict of interest.

Special issue statement. This article is part of the special issue "The 4.2 ka BP climatic event". It is a result of "The 4.2 ka BP Event: An International Workshop", Pisa, Italy, 10–12 January 2018.

Acknowledgements. This study was supported by the NSFC (41502166), NSFC (41731174), NSF (1702816), the China Postdoctoral Science Foundation (2015M580832), the State Key Laboratory of Loess and Quaternary Geology (SKLLQG1046), the Key Laboratory of Karst Dynamics, Ministry of Land and Resources of the People's Republic of China (MLR), GZAR (KDL201502), and the Shaanxi Science Fund for Distinguished Young Scholars (2018JC-023).

Edited by: Giovanni Zanchetta
Reviewed by: two anonymous referees

References

Baker, A., Ito, E., Smart, P. L., and McEwan, R. F.: Elevated and variable values of ^{13}C in speleothems in a British cave system, Chem. Geol., 136, 263–270, 1997.

Baldini, J., McDermott, F., Baker, A., Baldini, L., Mattey, D., and Railsback, L. B.: Biomass effects on stalagmite growth and isotope ratios: A 20th century analogue from Wiltshire, England, Earth Planet. Sc. Lett., 240, 486–494, 2005.

Bar-Matthews, M. and Ayalon, A.: Mid-Holocene climate variations revealed by high-resolution speleothem records from Soreq Cave, Israel and their correlation with cultural changes, Holocene, 21, 163–171, 2011.

Berkelhammer, M., Sinha, A., Stott, L., Cheng, H., Pausata, F. S., and Yoshimura, K.: An abrupt shift in the Indian monsoon 4000 years ago, Geophys. Monogr. Ser, 198, 75–87, 2012.

Bond, G., Kromer, B., Beer, J., Muscheler, R., Evans, M. N., Showers, W., Hoffmann, S., Lotti-Bond, R., Hajdas, I., and Bonani, G.: Persistent solar influence on North Atlantic climate during the Holocene, Science, 294, 2130–2136, 2001.

Booth, R. K., Jackson, S. T., Forman, S. L., Kutzbach, J. E., Bettis Iii, E., Kreigs, J., and Wright, D. K.: A severe centennial-scale drought in midcontinental North America 4200 years ago and apparent global linkages, Holocene, 15, 321–328, 2005.

Breitenbach, S. F. M., Rehfeld, K., Goswami, B., Baldini, J. U. L., Ridley, H. E., Kennett, D. J., Prufer, K. M., Aquino, V. V., Asmerom, Y., Polyak, V. J., Cheng, H., Kurths, J., and Marwan, N.: COnstructing Proxy Records from Age models (COPRA), Clim. Past, 8, 1765–1779, https://doi.org/10.5194/cp-8-1765-2012, 2012.

Cai, Y., Tan, L., Cheng, H., An, Z., Edwards, R. L., Kelly, M. J., Kong, X., and Wang, X.: The variation of summer monsoon precipitation in central China since the last deglaciation, Earth Planet. Sc. Lett., 291, 21–31, 2010.

Cai, Y., Zhang, H., Cheng, H., An, Z., Edwards, R. L., Wang, X., Tan, L., Liang, F., Wang, J., and Kelly, M.: The Holocene Indian monsoon variability over the southern Tibetan Plateau and its teleconnections, Earth Planet. Sc. Lett., 335, 135–144, 2012.

Chen, F., Xu, Q., Chen, J., Birks, H. J. B., Liu, J., Zhang, S., Jin, L., An, C., Telford, R. J., and Cao, X.: East Asian summer monsoon precipitation variability since the last deglaciation, Sci. Rep., 5, 11186, https://doi.org/10.1038/srep11186, 2015.

Cheng, H., Edwards, R. L., Shen, C.-C., Polyak, V. J., Asmerom, Y., Woodhead, J., Hellstrom, J., Wang, Y., Kong, X., and Spötl, C.: Improvements in ^{230}Th dating, ^{230}Th and ^{234}U half-life values, and U–Th isotopic measurements by multi-collector inductively coupled plasma mass spectrometry, Earth Planet. Sc. Lett., 371, 82–91, 2013.

Cheng, H., Edwards, R. L., Sinha, A., Spötl, C., Yi, L., Chen, S., Kelly, M., Kathayat, G., Wang, X., Li, X., Kong, X., Wang, Y., Ning, Y., and Zhang, H.: The Asian monsoon over the past 640,000 years and ice age terminations, Nature, 534, 640–646, 2016.

Cheng, H., Edwards, R., Hoff, J., Gallup, C., Richards, D., and Asmerom, Y.: The half-lives of uranium-234 and thorium-230, Chem. Geol., 169, 17–33, 2000.

Chiang, J. C., Fung, I. Y., Wu, C.-H., Cai, Y., Edman, J. P., Liu, Y., Day, J. A., Bhattacharya, T., Mondal, Y., and Labrousse, C. A.: Role of seasonal transitions and westerly jets in East Asian paleoclimate, Quaternary Sci. Rev., 108, 111–129, 2015.

Cruz Jr, F. W., Burns, S. J., Karmann, I., Sharp, W. D., Vuille, M., and Ferrari, J. A.: A stalagmite record of changes in atmospheric circulation and soil processes in the Brazilian subtropics during the Late Pleistocene, Quaternary Sci. Rev., 25, 2749–2761, 2006.

Cullen, H. M., deMenocal, P. B., Hemming, S., Hemming, G., Brown, F. H., Guilderson, T., and Sirocko, F.: Climate change and the collapse of the Akkadian empire: Evidence from the deep sea, Geology, 28, 379–382, 2000.

De Choudens-Sanchez, V. and Gonzalez, L. A.: Calcite and aragonite precipitation under controlled instantaneous supersaturation: elucidating the role of $CaCO_3$ saturation state and Mg/Ca ratio

on calcium carbonate polymorphism, J. Sediment. Res., 79, 363–376, 2009.

DeMenocal, P. B.: Cultural responses to climate change during the late Holocene, Science, 292, 667–673, 2001.

Dong, J., Wang, Y., and Cheng, H.: A high-resolution stalagmite record of the Holocene East Asian monsoon from Mt Shennongjia, central China, Holocene, 20, 257–264, 2010.

Dong, J., Shen, C.-C., Kong, X., Wang, H.-C., and Jiang, X.: Reconciliation of hydroclimate sequences from the Chinese Loess Plateau and low-latitude East Asian Summer Monsoon regions over the past 14,500 years, Palaeogeogr. Palaeocl., 435, 127–135, 2015.

Dorale, J. A. and Liu, Z.: Limitations of Hendy test criteria in judging the paleoclimatic suitability of speleothems and the need for replication, J. Cave Karst Stud., 71, 73–80, 2009.

Dorale, J. A., Edwards, R. L., Ito, E., and Gonzalez, L. A.: Climate and vegetation history of the midcontinent from 75 to 25 ka: a speleothem record from Crevice Cave, Missouri, USA, Science, 282, 1871–1874, 1998.

Edwards, R. L., Chen, J., and Wasserburg, G.: ^{238}U-^{234}U-^{230}Th-^{232}Th systematics and the precise measurement of time over the past 500,000 years, Earth Planet. Sc. Lett., 81, 175–192, 1987.

Fairchild, I., Borsato, A., Tooth, A., Frisia, S., Hawkesworth, C., Huang, Y., McDermott, F., and Spiro, B.: Controls on trace element (Sr-Mg) compositions of carbonate cave waters: implications for speleothem climatic records, Chem. Geol., 166, 255–269, 2000.

Fairchild, I., Smith, C., Baker, A., Fuller, L., Spötl, C., Mattey, D., and McDermott, F.: Modification and preservation of environmental signals in speleothems, Earth Sci. Rev., 75, 105–153, 2006.

Fleitmann, D., Cheng, H., Badertscher, S., Edwards, R., Mudelsee, M., Göktürk, O. M., Fankhauser, A., Pickering, R., Raible, C., and Matter, A.: Timing and climatic impact of Greenland interstadials recorded in stalagmites from northern Turkey, Geophys. Res. Lett., 36, L19707, https://doi.org/10.1029/2009GL040050, 2009.

Frisia, S., Fairchild, I. J., Fohlmeister, J., Miorandi, R., Spötl, C., and Borsato, A.: Carbon mass-balance modelling and carbon isotope exchange processes in dynamic caves, Geochim. Cosmochim. Ac., 75, 380–400, 2011.

Gasse, F.: Hydrological changes in the African tropics since the Last Glacial Maximum, Quaternary Sci. Rev., 19, 189–211, 2000.

Genty, D., Baker, A., Massault, M., Proctor, C., Gilmour, M., Pons-Branchu, E., and Hamelin, B.: Dead carbon in stalagmites: carbonate bedrock paleodissolution vs. ageing of soil organic matter. Implications for ^{13}C variations in speleothems, Geochim. Cosmochim. Ac., 65, 3443–3457, 2001.

Genty, D., Blamart, D., Ouahdi, R., Gilmour, M., Baker, A., Jouzel, J., and Van-Exter, S.: Precise dating of Dansgaard–Oeschger climate oscillations in western Europe from stalagmite data, Nature, 421, 833–837, 2003.

Genty, D., Blamart, D., Ghaleb, B., Plagnes, V., Causse, C., Bakalowicz, M., Zouari, K., Chkir, N., Hellstrom, J., and Wainer, K.: Timing and dynamics of the last deglaciation from European and North African δ^{13}C stalagmite profiles – comparison with Chinese and South Hemisphere stalagmites, Quaternary Sci. Rev., 25, 2118–2142, 2006.

Hendy, C. H.: The isotopic geochemistry of speleothems – I. The calculation of the effects of different modes of formation on the isotopic composition of speleothems and their applicability as palaeoclimatic indicators, Geochim. Cosmochim. Ac., 35, 801–824, 1971.

Hu, C., Henderson, G., Huang, J., Xie, S., Sun, Y., and Johnson, K.: Quantification of Holocene Asian monsoon rainfall from spatially separated cave records, Earth Planet. Sc. Lett., 266, 221–232, 2008.

Huang, C. C., Pang, J., Zha, X., Zhou, Y., Su, H., and Li, Y.: Extraordinary floods of 4100–4000 a BP recorded at the Late Neolithic ruins in the Jinghe River gorges, Middle Reach of the Yellow River, China, Palaeogeogr. Palaeocl., 289, 1–9, 2010.

Huang, C. C., Pang, J., Zha, X., Su, H., and Jia, Y.: Extraordinary floods related to the climatic event at 4200 a BP on the Qishuihe River, middle reaches of the Yellow River, China, Quaternary Sci. Rev., 30, 460–468, 2011.

Jiang, X., He, Y., Shen, C., Kong, X., Li, Z., and Chang, Y.: Stalagmite-inferred Holocene precipitation in northern Guizhou Province, China, and asynchronous termination of the Climatic Optimum in the Asian monsoon territory, Chinese Sci. Bull., 57, 795–801, 2012.

Jiang, X., He, Y., Shen, C.-C., Li, Z., and Lin, K.: Replicated stalagmite-inferred centennial-to decadal-scale monsoon precipitation variability in southwest China since the mid Holocene, Holocene, 23, 841–849, 2013.

Jin, G. and Liu, D.: Mid-Holocene climate change in North China, and the effect on cultural development, Chinese Sci. Bull., 47, 408–413, 2002.

Li, T., Shen, C., Li, H., Li, J., Chiang, H., Song, S., Yuan, D., Lin, C., Gao, P., and Zhou, L.: Oxygen and carbon isotopic systematics of aragonite speleothems and water in Furong Cave, Chongqing, China, Geochim. Cosmochim. Ac., 75, 4140–4156, 2011.

Liu, F., and Feng, Z.: A dramatic climatic transition at $\sim$ 4000 cal. yr BP and its cultural responses in Chinese cultural domains, Holocene, 22, 1181–1197, 2012.

Ma, C., Zhu, C., Zheng, C., Wu, C., Guan, Y., Zhao, Z., Huang, L., and Huang, R.: High-resolution geochemistry records of climate changes since late-glacial from Dajiuhu peat in Shennongjia Mountains, Central China, Chinese Sci. Bull., 53, 28–41, 2008.

McDermott, F.: Palaeo-climate reconstruction from stable isotope variations in speleothems: a review, Quaternary Sci. Rev., 23, 901–918, 2004.

Meyer, K. W., Feng, W., Breecker, D. O., Banner, J. L., and Guilfoyle, A.: Interpretation of speleothem calcite δ^{13}C variations: Evidence from monitoring soil CO_2, drip water, and modern speleothem calcite in central Texas, Geochim. Cosmochim. Ac., 142, 281–298, 2014.

Noronha, A. L., Johnson, K. R., Southon, J. R., Hu, C., Ruan, J., and McCabe-Glynn, S.: Radiocarbon evidence for decomposition of aged organic matter in the vadose zone as the main source of speleothem carbon, Quaternary Sci. Rev., 127, 37–47, 2015.

Oster, J. L., Montanez, I. P., Guilderson, T. P., Sharp, W. D., and Banner, J. L.: Modeling speleothem δ^{13}C variability in a central Sierra Nevada cave using ^{14}C and ^{87}Sr / ^{86}Sr, Geochim. Cosmochim. Ac., 74, 5228–5242, 2010.

Peng, Y., Xiao, J., Nakamura, T., Liu, B., and Inouchi, Y.: Holocene East Asian monsoonal precipitation pattern revealed by grain-

size distribution of core sediments of Daihai Lake in Inner Mongolia of north-central China, Earth Planet. Sc. Lett., 233, 467–479, 2005.

Railsback, L. B.: A comparison of growth rate of late Holocene stalagmites with atmospheric precipitation and temperature, and its implications for paleoclimatology, Quaternary Sci. Rev., 187, 94–111, 2018.

Railsback, L. B., Liang, F., Brook, G., Voarintsoa, N. R. G., Sletten, H. R., Marais, E., Hardt, B., Cheng, H., and Edwards, R. L.: The timing, two-pulsed nature, and variable climatic expression of the 4.2 ka event: A review and new high-resolution stalagmite data from Namibia, Quaternary Sci. Rev., 186, 78–90, 2018.

Ruan, J., Kherbouche, F., Genty, D., Blamart, D., Cheng, H., Dewilde, F., Hachi, S., Edwards, R. L., Régnier, E., and Michelot, J.-L.: Evidence of a prolonged drought ca. 4200 yr BP correlated with prehistoric settlement abandonment from the Gueldaman GLD1 Cave, Northern Algeria, Clim. Past, 12, 1–14, https://doi.org/10.5194/cp-12-1-2016, 2016.

Tan, L., An, Z., Cai, Y., and Long, H.: The hydrological exhibition of 4200 aBP event in China and its global linkages, Geol. Rev., 54, 94–104, 2008 (in Chinese with English abstract).

Tan, L., Cai, Y., Cheng, H., Edwards, L. R., Gao, Y., Xu, H., Zhang, H., and An, Z.: Centennial-to decadal-scale monsoon precipitation variations in the upper Hanjiang River region, China over the past 6650 years, Earth Planet. Sc. Lett., 482, 580–590, 2018a.

Tan, L., Shen, C.-C., Cai, Y., Cheng, H., and Edwards, R. L.: Great flood in the middle-lower Yellow River reaches at 4000 a BP inferred from accurately-dated stalagmite records, Sci Bull., 63, 206–208, 2018b.

Tan, M. and Cai, B.: Preliminary calibration of stalagmite oxygen isotopes from eastern monsoon China with Northern Hemisphere temperatures, Pages News, 13, 16–17, 2005.

Tan, M.: Circulation background of climate patterns in the past millennium: Uncertainty analysis and re-reconstruction of ENSO-like state, Sci. China Earth Sci., 59, 1225–1241, 2016.

Tan, M.: Circulation effect: climatic significance of the short term variability of the oxygen isotopes in stalagmites from monsoonal China – dialogue between paleoclimate records and modern climate research, Quaternary Sci., 29, 851–862, 2009 (in Chinese with English abstract).

Tan, M.: Circulation effect: response of precipitation $\delta^{18}O$ to the ENSO cycle in monsoon regions of China, Clim. Dynam., 42, 1067–1077, 2014.

Thompson, L. G., Mosley-Thompson, E., Davis, M. E., Henderson, K. A., Brecher, H. H., Zagorodnov, V. S., Mashiotta, T. A., Lin, P.-N., Mikhalenko, V. N., and Hardy, D. R.: Kilimanjaro ice core records: evidence of Holocene climate change in tropical Africa, Science, 298, 589–593, 2002.

Tian, S.-F. and Yasunari, T.: Climatological aspects and mechanism of spring persistent rains over central China, J. Meteorol. Soc. Jpn. Ser. II, 76, 57–71, 1998.

Tremaine, D. M., Froelich, P. N., and Wang, Y.: Speleothem calcite farmed in situ: Modern calibration of $\delta^{18}O$ and $\delta^{13}C$ paleoclimate proxies in a continuously-monitored natural cave system, Geochim. Cosmochim. Ac., 75, 4929–4950, 2011.

Walker, M., Head, M. j., Berkelhammer, M., Björck, s., Cheng, h., Cwynar, L., Fisher, D., Gkinis, V., Long, A., Lowe, J., Newnham, R., Olander, R. S., Weiss, H.: Formal ratification of the subdivision of the Holocene Series/Epoch (Quaternary System/Period): two new Global Boundary Stratotype Sections and Points (GSSPs) and three new stages/subseries, IUGS, Episodes, 1–11, https://doi.org/10.18814/epiiugs/2018/018016, 2018.

Wan, R. and Wu, G.: Mechanism of the spring persistent rains over southeastern China, Sci. China Ser. D, 50, 130–144, 2007.

Wan, R. and Wu, G.: Temporal and spatial distributions of the spring persistent rains over Southeastern China, J. Meteorol. Res., 23, 598–608, 2009.

Wan, R., Wang, T., and Wu, G.: Temporal variations of the spring persistent rains and South China Sea sub-high and their correlations to the circulation and precipitation of the East Asian Summer Monsoon, J. Meteorol. Res., 22, 530–537, 2008.

Wang, B. and Lin, H.: Rainy season of the Asian–Pacific summer monsoon, J. Clim., 15, 386–398, 2002.

Wang, Y., Cheng, H., Edwards, R., An, Z., Wu, J., Shen, C., and Dorale, J.: A high-resolution absolute-dated late Pleistocene monsoon record from Hulu Cave, China, Science, 294, 2345–2348, 2001.

Wang, Y., Cheng, H., Edwards, R., He, Y., Kong, X., An, Z., Wu, J., Kelly, M., Dykoski, C., and Li, X.: The Holocene Asian monsoon: links to solar changes and North Atlantic climate, Science, 308, 854–857, 2005.

Weiss, H. and Bradley, R. S.: What drives societal collapse?, Science, 291, 609–610, 2001.

Weiss, H., Courty, M.-A., Wetterstrom, W., Guichard, F., Senior, L., Meadow, R., and Curnow, A.: The genesis and collapse of third millennium north Mesopotamian civilization, Science, 261, 995–1004, 1993.

Wong, C. I. and Breecker, D. O.: Advancements in the use of speleothems as climate archives, Quaternary Sci. Rev., 127, 1–18, 2015.

Wu, J., Wang, Y., and Dong, J.: Changes in East Asian summer monsoon during the Holocene recorded by stalagmite $\delta^{18}O$ records from Liaoning Province, Quaternary Sci., 31, 990–998, 2011 (in Chinese with English abstract).

Wu, L., Zhu, C., Ma, C., Li, F., Meng, H., Liu, H., Li, L., Wang, X., Sun, W., and Song, Y.: Mid-Holocene palaeoflood events recorded at the Zhongqiao Neolithic cultural site in the Jianghan Plain, middle Yangtze River Valley, China, Quaternary Sci. Rev., 173, 145–160, 2017.

Xiao, J., Si, B., Zhai, D., Itoh, S., and Lomtatidze, Z.: Hydrology of Dali lake in central-eastern Inner Mongolia and Holocene East Asian monsoon variability, J. Paleolimnol., 40, 519–528, 2008.

Xiao, J., Zhang, S., Fan, J., Wen, R., Xu, Q., Inouchi, Y., and Nakamura, T.: The 4.2 ka event and its resulting cultural interruption in the Daihai Lake basin at the East Asian summer monsoon margin, Quatern. Int., https://doi.org/10.1016/j.quaint.2018.06.025, 2018a.

Xiao, J., Zhang, S., Fan, J., Wen, R., Zhai, D., Tian, Z., and Jiang, D.: The 4.2 ka BP event: multi-proxy records from a closed lake in the northern margin of the East Asian summer monsoon, Clim. Past, 14, 1417–1425, https://doi.org/10.5194/cp-14-1417-2018, 2018b.

Xu, H., Hong, Y., Lin, Q., Zhu, Y., Hong, B., and Jiang, H.: Temperature responses to quasi-100-yr solar variability during the past 6000 years based on $\delta^{18}O$ of peat cellulose in Hongyuan, eastern Qinghai–Tibet plateau, China, Palaeogeogr. Palaeocl., 230, 155–164, 2006.

Yan, M., Liu, J., and Ning, L.: Physical processes of cooling and megadrought in 4.2 ka BP event: results from TraCE-21 ka simulations, Clim. Past Discuss., https://doi.org/10.5194/cp-2018-131, in review, 2018.

Yao, F., Ma, C., Zhu, C., Li, J., Chen, G., Tang, L., Huang, M., Jia, T., and Xu, J.: Holocene climate change in the western part of Taihu Lake region, East China, Palaeogeogr. Palaeocl., 485, 963–973, 2017.

Yao, T. and Thompson, L. G.: Trends and features of climatic changes in the past 5000 years recorded by the Dunde ice core, Ann. Glaciol., 16, 21–24, 1992.

Zhang, E., Zhao, C., Xue, B., Liu, Z., Yu, Z., Chen, R., and Shen, J.: Millennial-scale hydroclimate variations in southwest China linked to tropical Indian Ocean since the Last Glacial Maximum, Geology, 45, 435–438, 2017.

Zhang, G., Zhu, C., Wang, J., Zhu, G., Ma, C., Zheng, C., Zhao, L., Li, Z., Li, L., and Jin, A.: Environmental archaeology on Longshan Culture (4500–4000 a BP) at Yuhuicun Site in Bengbu, Anhui Province, J. Geogr. Sci., 20, 455–468, 2010.

Zhang, H., Cai, Y., Tan, L., Cheng, H., Qin, S., An, Z., Edwards, R. L., and Ma, L.: Large variations of δ^{13}C values in stalagmites from southeastern China during historical times: implications for anthropogenic deforestation, Boreas, 44, 511–525, 2015.

Zhang, H., Cai, Y., Tan, L., Qin, S., and An, Z.: Stable isotope composition alteration produced by the aragonite-to-calcite transformation in speleothems and implications for paleoclimate reconstructions, Sediment. Geol., 309, 1–14, 2014.

Zhang, H., Cheng, H., Spötl, C., Cai, Y., Sinha, A., Tan, L., Yi, L., Yan, H., Kathayat, G., Ning, Y., Li, X., Zhang, F., Zhao, J., and Edwards, R. L.: A 200-year annually laminated stalagmite record of precipitation seasonality in southeastern China and its linkages to ENSO and PDO, Sci. Rep., 8, 12344, https://doi.org/10.1038/s41598-018-30112-6, 2018.

Zhang, M., Lin, Y., Zhu, X., Qin, J., Yang, Y., and Luo, G.: The records of climatic change from a stalagmite during the late time of the middle Holocene in Ninglang area, Yunnan, Marine Geology & Quaternary Geology, 26, 35–40, 2006 (in Chinese with English abstract).

Zhang, M., Yuan, D. X., Lin, Y., Qin, J., Bin, L., Cheng, H., and Edwards, R. L.: A 6000-year high-resolution climatic record from a stalagmite in Xiangshui Cave, Guilin, China, Holocene, 14, 697–702, 2004.

Zhang, W. and Wu, J.: Ecological response of δ^{13}C to Holocene climate changes from stalagmite record in Nuanhe Cave, Liaoning, Marine Geology & Quaternary Geology, 32, 147–154, 2012 (in Chinese with English abstract).

Zhao, L., Ma, C., Leipe, C., Long, T., Liu, K.-b., Lu, H., Tang, L., Zhang, Y., Wagner, M., and Tarasov, P. E.: Holocene vegetation dynamics in response to climate change and human activities derived from pollen and charcoal records from southeastern China, Palaeogeogr. Palaeocl., 485, 644–660, 2017.

Zhao, Y., Chen, F., Zhou, A., Yu, Z., and Zhang, K.: Vegetation history, climate change and human activities over the last 6200 years on the Liupan Mountains in the southwestern Loess Plateau in central China, Palaeogeogr. Palaeocl., 293, 197–205, 2010.

Zhong, W., Cao, J., Xue, J., and Ouyang, J.: A 15,400-year record of climate variation from a subalpine lacustrine sedimentary sequence in the western Nanling Mountains in South China, Quaternary Res., 84, 246–254, 2015.

Zhong, W., Wei, Z., Chen, Y., Shang, S., Xue, J., Ouyang, J., Cao, J., Chen, B., and Zhu, C.: A 15.4-ka paleoclimate record inferred from δ^{13}C and δ^{15}N of organic matter in sediments from the sub-alpine Daping Swamp, western Nanling Mountains, South China, J. Paleolimnol., 57, 127–139, 2017.

Zhong, W., Xue, J., Cao, J., Zheng, Y., Ma, Q., Ouyang, J., Cai, Y., Zeng, Z., and Liu, W.: Bulk organic carbon isotopic record of lacustrine sediments in Dahu Swamp, eastern Nanling Mountains in South China: Implication for catchment environmental and climatic changes in the last 16,000 years, J. Asian Earth Sci., 38, 162–169, 2010a.

Zhong, W., Xue, J., Zheng, Y., Ma, Q., Cai, Y., Ouyang, J., Xu, L., Zhou, S., and Yu, X.: Variations of monsoonal precipitation over the last 16,000 years in the eastern Nanling Mountains, South China, J. Paleolimnol., 44, 177–188, 2010b.

Zhong, W., Xue, J., Zheng, Y., Ouyang, J., Ma, Q., Cai, Y., and Tang, X.: Climatic changes since the last deglaciation inferred from a lacustrine sedimentary sequence in the eastern Nanling Mountains, south China, J. Quaternary Sci., 25, 975–984, 2010c.

Zhou, J., Wang, S., and Lv, J.: Climatic and environmental changes from the sediment record of Erhai Lake over the past 10000 years, J. Lake Sci., 2, 104–110, 2003 (in Chinese with English abstract).

Zhou, W., Lu, X., Wu, Z., Deng, L., Jull, A., Donahue, D., and Beck, W.: Peat record reflecting Holocene climatic change in the Zoigê Plateau and AMS radiocarbon dating, Chinese Sci. Bull., 47, 66–70, 2002.

Zhou, W., Yu, X., Jull, A. T., Burr, G., Xiao, J., Lu, X., and Xian, F.: High-resolution evidence from southern China of an early Holocene optimum and a mid-Holocene dry event during the past 18,000 years, Quaternary Res., 62, 39–48, 2004.